Journal of Fluids and Structures (2001) **15,** 587–596
doi:10.1006/jfls.2000.0354, available online at http://www.idealibrary.com on IDEAL®

FLOW PAST A BLUFF BODY WITH A WAVY STAGNATION FACE

R. M. Darekar and S. J. Sherwin

Department of Aeronautics, Imperial College of Science, Technology and Medicine London, SW7 2BY, U.K.

(Received 7 September 2000, and in final form 15 November 2000)

Numerical investigations have been performed to study the flow past square-section cylinders with a spanwise geometric deformation leading to a stagnation face with a sinusoidal waviness. The computations were performed using a spectral/*hp* element solver over a range of Reynolds numbers from 10 to 500. Starting from fully developed shedding past a straight cylinder at a Reynolds number of 100, a sufficiently high waviness is impulsively introduced resulting in the stabilization of the the near-wake to a time-independent state. The steady nature of the near-wake is associated with a reduction in total drag of about 16% at a Reynolds number of 100 as compared with a straight, non-wavy cylinder. Further increases in the amplitude of the waviness lead to the emergence of hairpin vortices from the near-wake region, similar to the wake of a sphere at low Reynolds numbers. At higher Reynolds numbers, the drag reduction increases substantially, e.g. at a Reynolds number of 500 it is 34%, principally due to the increase in drag of the nonwavy cylinder. Alternative methods based on three-dimensional forms of bleed are investigated to suppress the von-Kármán vortex street of a straight, non-wavy cylinder.

1. INTRODUCTION

To reduce the drag and weaken the vortex shedding of two-dimensional bluff bodies, three-dimensional disturbances can be introduced into the base geometry. Tanner (1972) introduced a broken separation line along the trailing edge of a blunt aerofoil. He applied a stepwise deformation to the trailing edge and observed that by increasing the depth of the steps, larger base drag reductions are obtained. The maximum drag reduction obtained using this method was 64%. The study of this drag reduction technique (segmented trailing edge) was then continued by Rodriguez (1991) and Petrusma & Gai (1994).

Bearman & Tombazis (1993) and Tombazis & Bearman (1997) investigated the three-dimensional features of the wake behind a blunt-based model with a wavy trailing edge at a Reynolds number of 40 000. They observed that the introduction of a spanwise waviness at the trailing edge fixed the positions of vortex dislocations along the span of the body. Increasing the wave steepness, defined as the ratio of peak-to-peak wave height divided by the wavelength, increased the base pressure which resulted in a drag reduction. The maximum drag reduction of 34% at a Reynolds number of 40 000 occurred for a wave steepness of 0.14. Based on these facts, they concluded that encouraging the formation of dislocations in the wake reduces the drag.

More recently Bearman & Owen (1998*a*, *b*) continued the above work by applying the waviness at the leading edge of a rectangular cross-section body. They observed that a mild disturbance (wave steepness of only 0·06–0·09) resulted in the complete suppression of

0889–9746/01/040587 + 10 $35.00/0

vortex shedding and substantial drag reduction of at least 30% at a Reynolds number of 40 000.

The aim of the current work is to carry out well-resolved numerical simulations of the flow past three-dimensional bluff bodies with a sinusoidal stagnation surface. The geometries used in this work have both sinusoidal front and rear faces. In the work of Bearman & Owen (1998*a*, *b*), only the front face was wavy for the rectangular cross-section bodies. However, in their experiments, similar results were also obtained with a flat plate which had both wavy front and rear faces. This latter result would suggest that the wavy trailing edge does not influence the qualitative observations made during the experiments of Bearman & Owen (1998*a*, *b*).

This paper is outlined as follows. Section 2 details the problem definition and introduces the nondimensional parameters as well as the numerical method. In Section 3, we present the main results of the effect of varying the Reynolds number for a cylinder with a constant amplitude of waviness. In addition, the effects of various forms of three-dimensional bleed on the wake topology of a straight, nonwavy cylinder are investigated.

2. PROBLEM DEFINITION AND SIMULATION METHOD

We are interested in the flow past a square-section cylinder with a waviness in both the front and rear faces as shown in Figure 1. The wavy cylinder is defined by the peak-to-peak wave height W, the wavelength λ and the base height D. The free-stream velocity U_∞ is aligned with the x-axis (streamwise direction), the span of the cylinder is aligned to the z-axis (spanwise or cross-flow direction) and finally the y-axis will be denoted as the vertical direction. We define the Reynolds number based on the base height D as $\mathrm{Re} = U_\infty D/\nu$, where ν is the kinematic viscosity of the fluid. The maximum denotes the most upstream cross-section (peak), while the minimum denotes the most downstream cross-section (valley). Furthermore, the waviness of the centreline (defined as a line going through the centroid of the body along the span) can be expressed mathematically in the following form:

$$\xi(z) = -\frac{W}{2}\cos(2\pi z/\lambda). \tag{1}$$

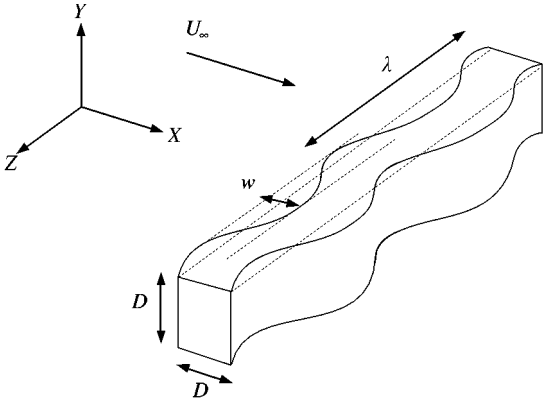

Figure 1. Schematic of the cylinder with the waviness at both the leading and trailing edge surfaces.

2.1. Dimensionless Length Scales

In contrast to the standard flow past a non-wavy cylinder, we have now introduced two extra length scales: W and λ. Whilst the non-wavy case can be completely characterized by the Reynolds number based upon the base height D, we now have a further two independent length parameters that we choose to define as W/λ and λ/D.

Differentiating equation (1) with respect to z gives an expression for the slope of the waviness $\mathrm{d}\xi/\mathrm{d}z$:

$$\frac{\mathrm{d}\xi}{\mathrm{d}z} = \pi\frac{W}{\lambda}\sin(2\pi z/\lambda) = A_s\sin(2\pi z/\lambda), \tag{2}$$

where $A_s = \pi W/\lambda$ is the maximum magnitude of the slope and depends on W/λ which is defined as the wave steepness (Bearman & Owen 1998*a*, *b*). The slope of the waviness which is proportional to the wave steepness reaches a maximum value of A_s at the inflection points $z = \lambda/4, \quad 3\lambda/4$.

2.2 Simulation Method

A parallel spectral element code $\mathcal{N}\varepsilon\kappa\mathcal{T}\alpha r$ (Sherwin & Karniadakis 1995) was employed to solve the three-dimensional incompressible Navier–Stokes equations. Spectral element methods have been widely used in the past for the prediction of bluff body flows due to their high spatial accuracy. Solution refinement can be obtained either by refining the mesh (h-refinement) or increasing the polynomial order P (P-refinement). To incorporate the wavy geometries, a geometric mapping is introduced as previously adopted by Newman (1996) and Evangelinos (1999). Application of the mapping to the Navier–Stokes equations leads to the modified set of equations:

$$\frac{\partial\mathbf{u}}{\partial t} + (\mathbf{u}\cdot\nabla)\mathbf{u} = -\nabla p + \frac{1}{\mathrm{Re}}\nabla^2\mathbf{u} + \mathbf{A}(\mathbf{u}, p, \boldsymbol{\xi}),$$

$$\nabla\cdot\mathbf{u} = 0, \tag{3}$$

where $\mathbf{A}(\mathbf{u}, p, \boldsymbol{\xi}) = [A_x, A_y, A_z]^{\mathrm{T}}$ is the d'Alembert forcing term which as reported in Darekar & Sherwin (2001) has nonzero inviscid contributions of the form

$$A_z = \pi\frac{W}{\lambda}\sin(2\pi z/\lambda)\frac{\partial p}{\partial x}, \tag{4}$$

$$\mathrm{A}_x = \pi\frac{W}{\lambda}\sin(2\pi z/\lambda)\frac{\partial p}{\partial z} - \pi^2\left(\frac{W}{\lambda}\right)^2\sin^2(2\pi z/\lambda)\frac{\partial p}{\partial x} - 2w^2\pi^2\frac{W}{\lambda^2}\cos(2\pi z/\lambda). \tag{5}$$

3. RESULTS AND DISCUSSION

3.1. Parameter Space Study

In Darekar & Sherwin (2001), the wavelength λ and amplitude W of the waviness were varied at $\mathrm{Re} = 100$ introducing different degrees of geometric three dimensionality in the wake. From consideration of the wake topology in terms of the Jeong & Hussain (1995) identification criteria and force characteristics, the effect of introducing a wavy stagnation face was classified into five distinct regimes. A summary of the parameter space study is shown in Figure 2.

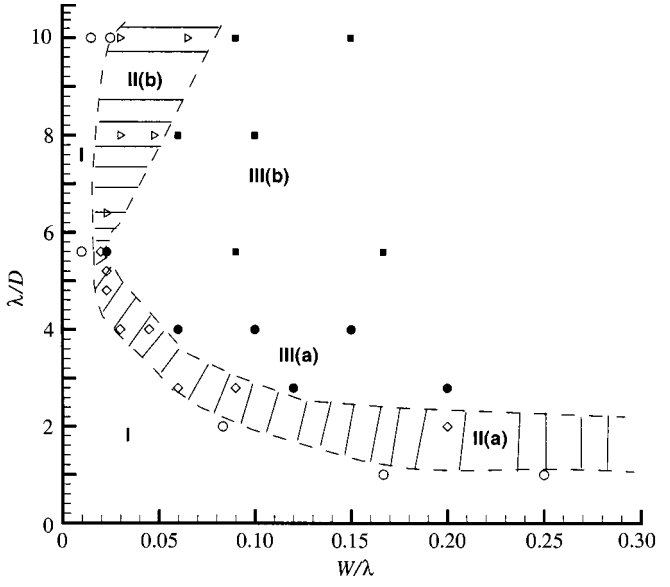

Figure 2. Summary of the parameter space study: λ/D versus W/λ at Re = 100. ○, regime I; ◇, regime II (type A); ▷, regime II (type B); ●, regime III (type A); ■, regime III (type B). From Darekar & Sherwin (2000).

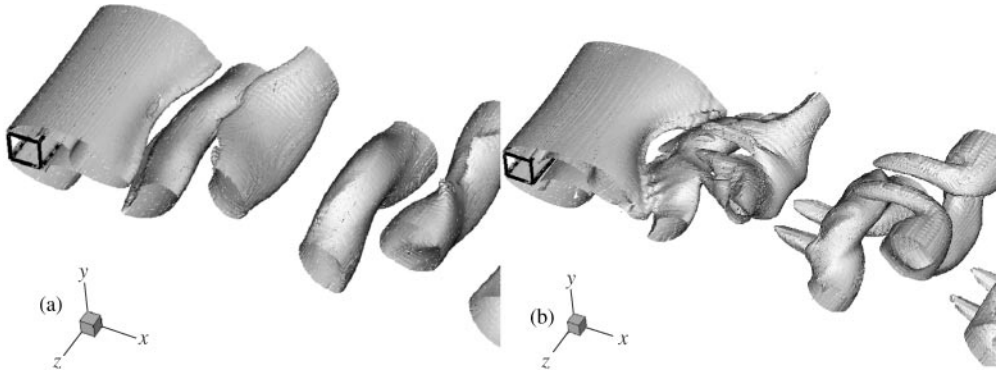

Figure 3. Perspective view from above showing the three-dimensional wake: (a) regime I; (b) regime II (type A).

For a mild geometric waviness we obtain regime I, where the formation of the wake at the base of the cylinder is mildly three dimensional and the force history is similar to the straight cylinder. However, as the wake evolves further downstream there is a discernible deformation of the spanwise Kármán vortices [see Figure 3(a)].

For a slightly higher level of waviness we obtain a transitional regime denoted as regime II. In this regime the effects of the geometric waviness in the formation region are more dominant. A large spanwise curvature appears in the top and bottom shear layers and an associated drop occurs in mean drag and the root-mean-square of the lift. Further downstream, we observe the formation of streamwise vortices associated with the sinusoidal spanwise deformation of the distorted Kármán vortices. Within this transitional regime II, we make a further distinction between normalized wavelengths above and below $\lambda/D \approx 5{\cdot}6$.

For $\lambda/D \leq 5{\cdot}6$, denoted as regime II (type A), we observe a time periodic state with a single frequency where streamwise vortices occur in the braids and connect adjacent Kármán vortices [see Figure 3(b)]. These streamwise vortices have some analogy with the streamwise structures of the mode A instability (see Williamson 1996). However, for $\lambda/D > 5.6$, denoted as regime II (type B), we observe a beating phenomenon where the wake topology alternates between a mildly three-dimensional state similar to regime I and a highly three-dimensional state similar to regime II (type A).

Finally, when the amplitude of the waviness is sufficiently large, we obtain a near-base region which is completely steady leading to a significant reduction in mean drag and the lift tending to zero. This region of maximal drag reduction is denoted by regime III and within this regime, there is no evidence of a Kármán vortex wake. Once again we can identify two sub-regimes. In the first case, regime III (type A), the flow is completely steady and has only been observed for $\lambda/D \leq 5{\cdot}6$. It is in regime III (type A) that the most significant drag reduction occurs. The wake topology is similar to that shown in Figure 5(a). However, when $\lambda/D > 5{\cdot}6$, hairpin vortices are shed periodically from the almost steady near-base region. In this regime, defined as regime III (type B), a small unsteadiness appears in the near-wake due to the shedding of these hairpin vortices. We note that the wake topology of the hairpin vortices in regime III (type B) resembles that of a sphere at low Reynolds numbers [see Figure 5(b)]. It was shown that the smallest wave steepness W/λ to force the flow into regime III (type A) occurs at around a value of $\lambda/D \approx 5{\cdot}6$. This wavelength has a similar length scale as the mode A transition of the wake of a straight, nonwavy square section cylinder and the primary spacing of same-sign vortices in a Kármán vortex street.

3.2. Reynolds Number Effect

The effect of the Reynolds number on the forces and wake topology of the wavy cylinder is investigated for the particular case of $(\lambda/D, W/\lambda) = (5{\cdot}6, 0{\cdot}167)$. The numerical simulations were performed over a range of Reynolds numbers from 10 to 500 and are compared with experimental data for the straight and wavy bodies up to a Reynolds number of 40 000. The results for the total drag coefficient against the Reynolds number are summarized in Figure 4.

For the straight cylinder, at low Reynolds numbers the flow is steady and a pair of symmetric vortices forms in the near-wake. In this regime, the drag is relatively high and has a strong component due to skin friction from the boundary layer. For example, at $\mathrm{Re} = 10$, the total drag coefficient is 3·20, 32% of which is due to wall shear stresses. As the Reynolds number is increased, the shear stress component of the total drag coefficient decreases and the length of the closed recirculating region increases; e.g at $\mathrm{Re} = 40$, the total drag coefficient is reduced to 1·71 and only 16% is due to skin friction.

At a critical Reynolds number Re_1, the steady flow becomes unstable and bifurcates to a two-dimensional time-periodic flow, resulting in the well-known Kármán vortex street in the wake. This first transition, known as the primary instability, is the result of a Hopf bifurcation. For the square-section cylinder, the experimental value for Re_1 reported in Sohankar *et al.* (1997) is $\mathrm{Re}_1 = 47 \pm 2$, whereas previous numerical computations place the critical Reynolds number for the onset of vortex shedding near $\mathrm{Re}_1 = 51{\cdot}2$ (Sohankar *et al.* 1998) and $\mathrm{Re}_1 = 53$ (Kelkar & Patankar 1992), respectively. Beyond this critical Reynolds number, the drag coefficient deviates from the steady and symmetric curve as shown in Figure 4. An interesting flow pattern then develops on the top and bottom surfaces with increasing Reynolds number as shown in the simulations of Robichaux *et al.* (1999). In this work, they show that at low Reynolds numbers, the shear layers remain attached on the top

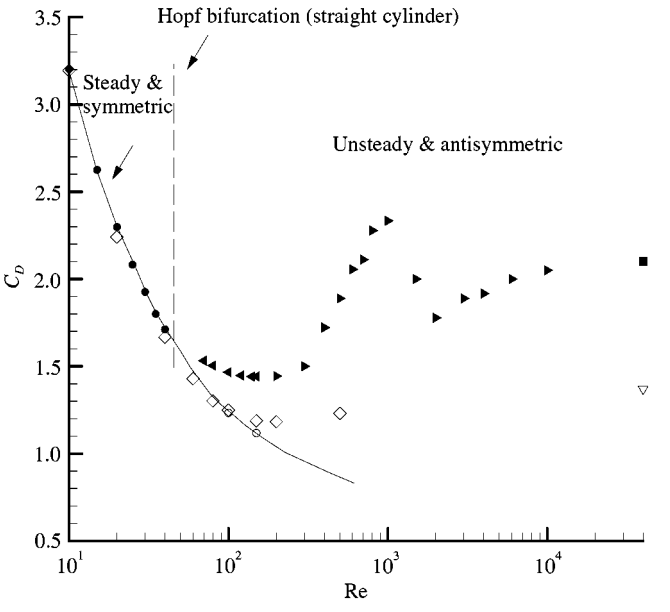

Figure 4. Drag coefficient against Reynolds number for the straight and wavy cylinders: ●, straight cylinder, Re = 10, 15, 20, 25, 30, 35, and 40 (steady flow); ◀, straight cylinder, Re = 70, 80, 100, 120, 140, and 150 (unsteady flow); ▶, straight cylinder, Re = 200 − 10,000 (experiments from Okajima 1995); ■, straight cylinder at Re = 40 000 (experiments from Owen 1997); ○, straight cylinder with symmetry boundary condition on the wake centre line to promote steady flow at Re = 100, 150; ◇, wavy cylinder, Re = 10, 20, 40, 60, 80, 100, 150, 200, and 500; ▽, wavy cylinder at Re = 40 000 (experiments from Owen 1997).

and bottom surfaces. The shear layers then separate from the trailing edge, forming the von-Kármán vortex street in the wake. As the Reynolds number is increased to around Re = 120, the shear layers separate from the leading edge but reattach a short distance downstream, thus forming small unsteady recirculating cells on the top and bottom surfaces. Finally, at around a Reynolds number of 150, the shear layers separate from the leading edge without reattachment. They also report that the two-dimensional wake becomes unstable to three-dimensional perturbations at around Re = 161, but the associated spanwise wavelength is not given. The onset of mode A for the square-section cylinder is given as Re = 162 ± 12. The lower bound of the onset of three dimensionality seems to be very close to the Reynolds number at which the flow separates from the leading edge without reattachment. From the experimental data of Okajima (1995), the total drag coefficient increases sharply from Re ≈ 200. It should be noted that this trend does not occur for the circular cylinder and is probably due to the fixed leading edge separation points. It is not yet clear why there is a large drop in the drag coefficient after Re = 1000 but it would seem to be due to the shear-layer transition (Okajima 2000). Further increasing the Reynolds number leads to a monotonic increase in the drag coefficient.

For the wavy body, the transition process is distinctively different. In the low Reynolds number regime, the drag coefficient is similar to that of the straight cylinder (see Figure 4). For example, at Re = 10, the total drag coefficient is 3·19, 32% of which is due to viscous shear stresses and at Re = 40, the total drag coefficient is 1·67 where 18% is due to skin friction. The wake topology is steady and symmetric which results in a net zero lift force.

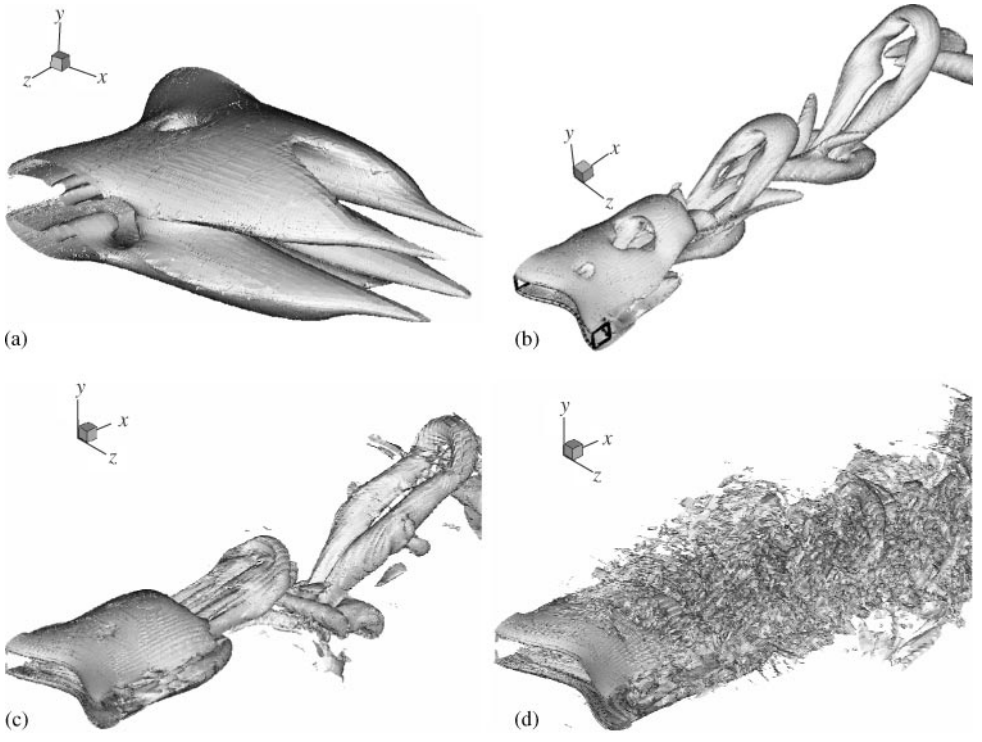

Figure 5. Perspective view showing the three-dimensional wake of the wavy cylinder $(\lambda/D, W/\lambda) = (5{\cdot}6, 0.1667)$ at (a) $\mathrm{Re} = 80$, (b) $\mathrm{Re} = 100$, (c) $\mathrm{Re} = 200$, and (d) $\mathrm{Re} = 500$.

The drag coefficient follows the steady and symmetric curve shown in Figure 4. Beyond the critical Reynolds number for the onset of vortex shedding of the straight cylinder ($\mathrm{Re}_1 \approx 47$), the three-dimensional wake remains steady and symmetric. The topology of the wake at $\mathrm{Re} = 80$ is shown in Figure 5(a). The drag coefficient continues to follow the steady and symmetric curve until $\mathrm{Re} \approx 100$. At around this critical Reynolds number, transition to unsteadiness occurs in the wake where the drag coefficient deviates from the steady and symmetric curve (see Figure 4). A staggered array of hairpin vortices emerge from the near-wake region as can be seen from Figure 5(b). The distinct structure of these hairpin vortices persists until $\mathrm{Re} = 200$, after which smaller scale instabilities are induced as shown by Figure 5(d) at $\mathrm{Re} = 500$. As can be seen, the wavy stagnation face has delayed the onset of unsteadiness to $\mathrm{Re} = 100$ and the antisymmetric mode has changed from a Kármán vortex street to a street composed of hairpin vortices, similar to the wake of a sphere at low Reynolds numbers.

Defining drag reduction with respect to the drag level of the straight cylinder, at $\mathrm{Re} = 80$ the drag reduction is about 13%, whereas at $\mathrm{Re} = 100$, 200 and 500, it is 16, 20 and 34%, respectively. It can be appreciated that the drag reduction at $\mathrm{Re} = 500$ has substantially increased from that at $\mathrm{Re} = 100$ and is comparable to the experiments of Owen (1997) at $\mathrm{Re} = 40\,000$. The increase in the drag reduction with increasing Reynolds number is principally due to the fact that for a straight, nonwavy cylinder, the shear layers separate from the leading edge from $\mathrm{Re} \approx 170$ whereas at $\mathrm{Re} = 100$ the shear layers remain attached until they separate from the trailing edge. Therefore, the leading edge separation leads to a higher drag for the straight, nonwavy cylinder. However, from the numerical simulation at higher Reynolds numbers, the asymptotic level of the drag coefficient of the wavy cylinder

does not change significantly from that at Re = 100 (see Figure 4). Therefore, the higher drag reduction, at higher Reynolds numbers, is mainly due to the increase in the drag coefficient of the straight, nonwavy cylinder.

3.3. Three-dimensional Bleed

Considering Section 2.2, we can introduce an alternative interpretation of the waviness as the d'Alembert flow past a straight, nonwavy cylinder.The spanwise forcing term A_z, given by equation (4), depends on the streamwise pressure gradient and the z-derivative of the shape of the waviness. The streamwise pressure gradient $\partial p/\partial x$ will be large near the stagnation face and will always be positive. The forcing term A_z will be positive between $0 < z < \lambda/2$ and negative between $\lambda/2 < z < \lambda$. This forcing, therefore, sets up a spanwise or cross-flow velocity component, w, along the leading edge surface going from a position corresponding to the maximum towards a position corresponding to the minimum of the wavy cylinder. In Darekar & Sherwin (2001), it was shown that the streamwise forcing term A_x, given by equation (5), is mainly dominated by the term $-\pi^2(W/\lambda)^2 \sin^2(2\pi z/\lambda)(1/\rho)(\partial p/\partial x)$, which is negative along the leading edge and reaches a maximum in the region of the inflection points. The streamwise forcing term, A_x, will thus slow down the two-dimensional u component of the velocity more significantly close to the inflection points.

These observations motivated the interpretation of the wavy stagnation face as a combination of promoting a cross-flow at the stagnation face and slowing down the flow near to the inflection points. To simulate this effect, the influence on the unsteady wake of a straight cylinder due to various forms of surface bleed has been investigated at a spanlength of $\lambda/D = 5{\cdot}6$ at Re = 100. Two types of bleed were imposed as boundary conditions on the cylinder surface: (i) a cross-flow bleed on the stagnation face, and (ii) a vertical bleed on the top and bottom surfaces. The following mathematical formulations were used for each of the three-dimensional forms of bleed:

(i) cross-flow bleed on the stagnation face, $w_{cr} = 0{\cdot}56 \sin(2\pi z/\lambda)(y - 0{\cdot}5)(y + 0{\cdot}5)$;
(ii) bleed on the top and bottom surfaces, $v_{tb} = \pm 0{\cdot}01\mathrm{e}^{-1000x^2}(1 + 200\,\mathrm{e}^{-(z-2{\cdot}8)^2})$.

The cross-flow bleed was specified on the whole stagnation face of the straight, nonwavy cylinder. The bleed has a sinusoidal variation in the spanwise z direction and a parabolic variation in the y direction. It reaches a local maximum of 0·14, i.e 14% of U_∞ at $z = 1{\cdot}4$, 4·2. The results showed that the near-wake was stabilized to a time-independent state. The wake topology is shown in Figure 6(a) and has strong qualitative similarities with that of the wavy cylinder in the steady regime [see Figure 5(a)]. The stabilization of the near-wake resulted in a drag reduction of about 15% and in a zero lift force.

The bleed on the top and bottom surface was specified by modifying the velocity boundary conditions on the top and bottom surfaces to $(u, v, w) = (0, \pm v_{tb}, 0)$. The distribution is exponential in both the streamwise x and spanwise z directions. A maximum velocity of about 2 occurs at the midspan of the cylinder. The topology of the wake is shown in Figure 6(b) and has strong similarities to the unsteady flow past the wavy cylinder at Re = 100 [see Figure 5(b)]. The lift force dropped to nearly zero and the drag reduction was equal to about 11%.

Current work is focusing on the minimum amount of bleed necessary to stabilize the near-wake. A comparison of this minimum amount of bleed will be done for the stagnation face cross-flow, the top and bottom surface bleed as well as the base bleed of the straight cylinder. It is anticipated that the stagnation face cross-flow will be the most effective means of stabilizing the near-wake as perturbations are introduced very early on in the shedding process and hence have a longer convective time to disrupt the shedding mechanism.

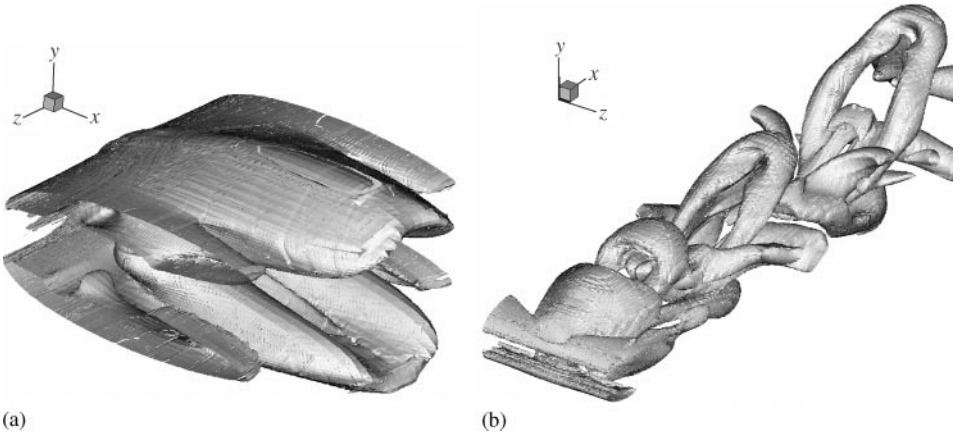

Figure 6. Perspective view showing the three-dimensional wake for the two forms of bleed: (a) on the stagnation face and (b) on the top and bottom surfaces.

4. CONCLUSION

It was shown that the wavy stagnation face delayed the onset of unsteadiness to Re $\approx$ 100 for the particular case of $(\lambda/D, W/\lambda) = (5{\cdot}6, 0{\cdot}167)$. In contrast to the standard von-Kármán vortex street of a straight cylinder, the unsteady wake of the wavy cylinder is composed of a staggered array of hairpin vortices, which is similar to the wake of sphere at low Reynolds numbers. The drag was found to be substantially lower than that of a straight cylinder. This drag reduction increased with increasing Reynolds number. Alternative methods, based on three-dimensional forms of bleed, have been shown to suppress the von-Kármán vortex street of a straight, nonwavy cylinder, leading to similar wake structures to that found for the wavy cylinder.

ACKNOWLEDGEMENTS

The authors would like to acknowledge several inspiring discussions and critical feedback from J. C. Owen, Prof. P. W. Bearman and Dr D. Barkley. The first author is supported by the Edmund Davis Trust fund awarded by the University of London. Computational resources were provided by the Computer Services for Academic Research (CSAR) under the EPSRC Grant Number GR/M08424 and the Imperial College Parallel Computing Centre.

REFERENCES

BEARMAN, P. W. & OWEN, J. C. 1998*a* Reduction of bluff-body drag and suppression of vortex shedding by the introduction of wavy separation lines. *Journal of Fluids and Structures* **12,** 123–130.

BEARMAN, P. W. & OWEN, J. C. 1998*b* Suppressing vortex shedding from bluff bodies by the introduction of wavy separation lines. In *Proceedings of the 1998 Conference on Bluff-Body Wakes and Vortex-Induced Vibration* (eds P. W. Bearman & C. H. K. Williamson), Paper No. 45, Ithaca, NY: Cornell University.

BEARMAN, P. W. & TOMBAZIS, N. 1993 The effect of three-dimensional imposed disturbances on bluff body near wake flows. *Journal of Wind Engineering & Industrial Aerodynamics* **49,** 339–350.

DAREKAR, R. M. & SHERWIN, S. J. 2001 Flow past a square-section cylinder with a wavy stagnation face. *Journal of Fluid Mechanics* **426,** 263–295.

EVANGELINOS, C. 1999 Parallel Spectral/hp Methods and Simulations of flow/structure Interactions. Ph.D. Thesis, Brown University, Providence, RI, U.S.A.

JEONG, J. & HUSSAIN, F. 1995 On the identification of a vortex. *Journal of Fluid Mechanics* **285,** 69–94.

KELKAR, K. M. & PATANKAR, S. V. 1992 Numerical prediction of vortex shedding behind a square cylinder. *International Journal for Numerical Methods in Fluids* **14,** 327–341.

NEWMAN, D. 1996 A computational study of fluid/structure interactions: flow-induced vibrations of a flexible cable. Ph.D. Thesis, Princeton University, Princeton, NJ, U.S.A.

OKAJIMA, A. 1995 Numerical analysis of the flow around an oscillating cylinder. In *Proceedings of the 6th International Conference on Flow-Induced Vibration*, pp. 159–166.

OKAJIMA, A. 2000 Private communication.

OWEN, J. C. 1997 The effect of three-dimensional disturbances on bluff body base drag. Final Year M. Eng. Project Report, Department of Aeronautics, Imperial College, London, U.K.

PETRUSMA, M. S. & GAI, S. L. 1994 The effect of geometry on the base pressure recovery of the segmented blunt trailing edges. *The Aeronautical Journal* **98,** 267–274.

ROBICHAUX, J., BALACHANDAR, S. & VANKA, S. P. 1999 Three-dimensional floquet instability of the wake of square cylinder. *Physics of Fluids* **11,** 560–578.

RODRIGUEZ, O. 1991 Base drag reduction by control of the three-dimensional unsteady vortical structures. *Experiments in Fluids* **11,** 218–226.

SHERWIN, S. J. & KARNIADAKIS, G. E. 1995 A triangular spectral element method: applications to the incompressible Navier–Stokes equations. *Computer Methods in Applied Mechanics and Engineering* **123,** 189–229.

SOHANKAR, A., NORBERG, C. & DAVIDSON, L. 1997 Numerical simulation of unsteady low-Reynolds number flow around rectangular cylinders at incidence. *Journal of Wind Engineering & Industrial Aerodynamics* **69,** 189–201.

SOHANKAR, A., NORBERG, C. & DAVIDSON, L. 1998 Low-Reynolds number flow around a square cylinder at incidence: study of blockage, onset of vortex shedding, and open boundary conditions. *International Journal for Numerical Methods in Fluids* **26,** 39–56.

TANNER, M. 1972 A method of reducing the base drag of wings with blunt trailing edge. *Aeronautical Quarterly* **23,** 15–23.

TOMBAZIS, N. & BEARMAN, P. W. 1997 A study of three-dimensional aspects of vortex shedding from a bluff body with a mild geometric disturbance. *Journal of Fluid Mechanics* **330,** 85–112.

WILLIAMSON, C. H. K. 1996 Three-dimensional wake transition. *Journal of Fluid Mechanics* **328,** 345–407.